

# MAKING RECONSTRUCTION FID PREDICTIVE OF DIFFUSION GENERATION FID

Tongda Xu<sup>1</sup>, Mingwei He<sup>1</sup>, Shady Abu-Hussein<sup>2</sup>, José Miguel Hernández-Lobato<sup>2\*</sup>,  
<sup>1</sup>Tsinghua University, <sup>2</sup>University of Cambridge

Haotian Zhang<sup>3</sup>, Kai Zhao<sup>3</sup>, Chao Zhou<sup>3</sup>, Ya-Qin Zhang<sup>1</sup>, Yan Wang<sup>1\*</sup>  
<sup>3</sup>Kuaishou Technology

## ABSTRACT

It is well known that the reconstruction FID (rFID) of a VAE is poorly correlated with the generation FID (gFID) of a latent diffusion model. We propose **interpolated FID (iFID)**, a simple variant of rFID that exhibits a strong correlation with gFID. Specifically, for each element in the dataset, we retrieve its nearest neighbor (NN) in the latent space and interpolate their latent representations. We then decode the interpolated latent and compute the FID between the decoded samples and the original dataset. Additionally, we refine the claim that rFID correlates poorly with gFID, by showing that rFID correlates with sample quality in the diffusion refinement phase, whereas iFID correlates with sample quality in the diffusion navigation phase. Furthermore, we provide an explanation for why iFID correlates well with gFID, and why reconstruction metrics are negatively correlated with gFID, by connecting to results in the diffusion generalization and hallucination. Empirically, iFID is the first metric to demonstrate a strong correlation with diffusion gFID, achieving Pearson linear and Spearman rank correlations  $\approx 0.85$ . The source code is provided in <https://github.com/tongdaxu/Making-rFID-Predictive-of-Diffusion-gFID>

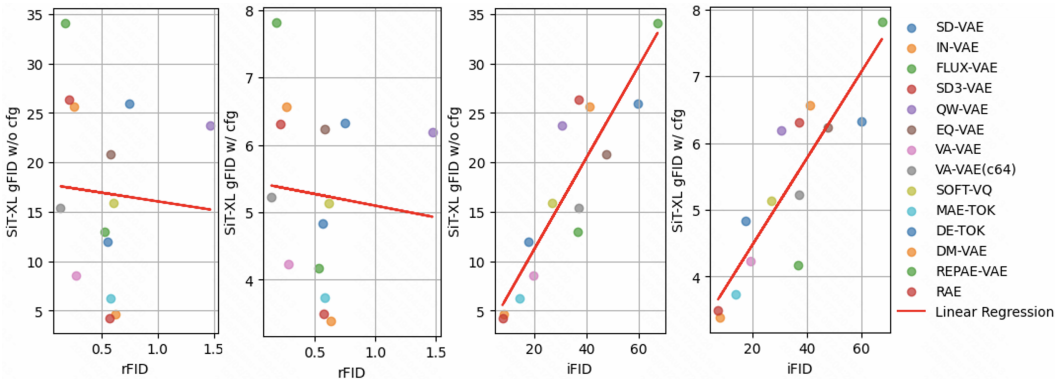


Figure 1: *Left two plots*: The rFID values of VAEs are uncorrelated, or even negatively correlated with, the gFID values of diffusion models. *Right two plots*: iFID metric exhibits a strong positive correlation with the gFID values of diffusion models.

## 1 INTRODUCTION

Variational autoencoders (VAEs) are foundational components of latent diffusion models (LDMs) (Rombach et al., 2022; Labs, 2024; Esser et al., 2024). In an LDM, a VAE first maps images into a latent space, after which a diffusion model is trained to generate samples in that space and decode

\*To whom correspondence should be addressed.

them back to pixel space. Thus, the quality of the VAE latent representation plays a critical role in the sample quality of the diffusion model.

VAEs are typically optimized and evaluated by reconstruction quality (Rombach et al., 2022; Esser et al., 2024), for example using reconstruction Fréchet Inception Distance (rFID) (Heusel et al., 2017). Intuitively, a VAE with better reconstruction preserves more details and should lead to better generation. However, a phenomenon termed the “reconstruction–generation dilemma” has recently been widely observed (Yao & Wang, 2025; Kouzelis et al., 2025; Ye et al., 2025; Skorokhodov et al., 2025; Chen et al., 2025b): VAEs with excellent rFID can result in poor generation FID (gFID). Conversely, VAEs with relatively worse rFID may have better generation performance.

In this work, we propose a simple variant of the rFID metric that correlates strongly with gFID, which we term **interpolated FID (iFID)**. Specifically, for each data point in the dataset, we identify its nearest neighbour in the latent space. We then interpolate the two latent, decode the interpolated sample to image. Finally, we compute the FID between these interpolated samples and the original dataset. In addition, we refine the common claim that rFID does not correlate well with gFID. Previous works (Liu et al., 2025a; Song et al., 2025) divide diffusion sampling into refinement and navigation phase, where sample’s detail and structure are determined respectively. We show that rFID reflects sample quality in the refinement phase, whereas iFID correlates with sample quality in the navigation phase. Further, by connecting to results in diffusion generalization and hallucination, we explain why iFID correlates well with diffusion sample quality but reconstruction correlates negatively with diffusion sample quality. Empirically, we find that iFID is strongly correlated with diffusion gFID with correlation  $\approx 0.85$ .

In summary, our contributions are as follows:

- We propose interpolated FID (iFID), a simple variant of rFID based on nearest-neighbour latent interpolation. iFID is the first metric shown to strongly correlate with diffusion gFID, achieving high Pearson and Spearman correlations across a wide range of models.
- We refine the statement that rFID correlates poorly with sample quality, by showing that rFID correlates with sample quality in refinement phase, while iFID correlates with sample quality in navigation phase.
- We provide an explanation for why iFID correlates well with generation performance and why reconstruction metrics do not, by relating to recent result in diffusion generalization and hallucination models.

## 2 PRELIMINARIES

### 2.1 LATENT DIFFUSION MODELS

The latent diffusion model (Rombach et al., 2022) consists of a variational autoencoder (VAE) (Kingma & Welling, 2013) that projects images into a latent space, and a diffusion model (Ho et al., 2020) that generates samples in this latent space. Let the source image be denoted as  $X \sim p(X)$ , and its latent as  $Z \sim q(Z|X)$ , where  $q(Z|X)$  is the variational posterior. The reconstructed image is given by  $\hat{X} = g(Z)$ , where  $g(\cdot)$  denotes the decoder. Given a Lagrange multiplier  $\lambda$  and a distortion measure  $\Delta(\cdot, \cdot)$ , the VAE minimizes a weighted combination of the KL divergence and the distortion:

$$\mathcal{L}_{\text{VAE}} = D_{\text{KL}}(q(Z|X)||\mathcal{N}(0, I)) + \lambda\Delta(X, \hat{X}). \quad (1)$$

The diffusion model is trained in the latent space to approximate the latent distribution  $p(Z)$ . The forward process of the diffusion model corresponds to constructing a Markov chain by incrementally adding noise associated with timestep  $t \in [0, T]$ . More specifically, given the diffusion parameters  $\alpha_t$  and  $\sigma_t^2$ , the conditional forward kernel of the forward diffusion process is

$$q(Z_t|Z) = \mathcal{N}(\alpha_t Z, \sigma_t^2 I). \quad (2)$$

The backward process of a diffusion model is described by the reverse stochastic differential equation (SDE) (Anderson, 1982). Sampling from the diffusion process involves simulating the reverse SDE from timestep  $T$  to 0 (Song et al., 2020) that depends only on the score  $\nabla_{Z_t} \log q(Z_t)$ . Therefore, the diffusion model is commonly parameterized by a score estimator  $s_\theta(Z_t, t)$  to approximate

$\nabla_{Z_t} \log q(Z_t)$ . The score estimator learns to minimize denoising score matching loss (Vincent, 2011):

$$\mathcal{L}_{\text{DSM}} = \mathbb{E} \|s_\theta(Z_t, t) - \nabla_{Z_t} \log q(Z_t|Z)\|_2. \quad (3)$$

## 2.2 REFINEMENT AND NAVIGATION PHASE OF DIFFUSION SAMPLING

Many previous works have shown that, for a diffusion sampling trajectory from timestep  $T$  to 0, most semantic features are determined when the timestep  $t$  is large, while only details are refined when  $t$  is small (Georgiev et al., 2023; Li & Chen, 2024; Song et al., 2025; Liu et al., 2025a). These two phases of sampling are known as the navigation phase and the refinement phase (Song et al., 2025; Liu et al., 2025a) of diffusion sampling.

## 2.3 RECONSTRUCTION-GENERATION DILEMMA

A well-known issue in LDMs is the “reconstruction-generation dilemma”. In early works on LDMs (Rombach et al., 2022; Esser et al., 2024), VAEs are optimized towards better reconstruction. Intuitively, VAEs with better reconstruction preserve more image details and facilitate improved learning in diffusion models. However, subsequent studies have pointed out that VAEs with better reconstruction performance are, counterintuitively, more challenging to train for diffusion models (Kouzelis et al., 2025; Ye et al., 2025; Skorokhodov et al., 2025; Chen et al., 2025a;c; Yao & Wang, 2025). As shown by (Yao & Wang, 2025; Yao et al., 2025), for VAEs without special regularization, a better rFID score typically leads to a worse gFID score. This phenomenon is referred to as the “reconstruction-generation dilemma”.

# 3 MAKING RECONSTRUCTION FID PREDICTIVE OF GENERATION FID

## 3.1 RECONSTRUCTION FID AND GENERATION FID

We denote the images in the validation dataset as  $x^{(1:N)}$ . The corresponding latent representations of these images are denoted as  $z^{(1:N)}$ . The Fréchet Inception Distance (FID) between two sets of images is represented as  $d_{\text{FID}}(\cdot, \cdot)$ . The decoder of the VAE is denoted by  $g(\cdot)$ , and the diffusion solver is denoted by  $\Phi(\cdot, \cdot)$ . The rFID and gFID can then be defined as follows:

$$\text{rFID} := d_{\text{FID}}(x^{(1:N)}, g(z^{(1:N)})), \quad (4)$$

$$\text{gFID} := d_{\text{FID}}(x^{(1:N)}, g(\Phi(\epsilon^{(1:M)}, T))), \text{ where } \epsilon^{(i)} \sim \mathcal{N}(0, I). \quad (5)$$

## 3.2 INTERPOLATED FID

It is well known that rFID does not correlate well with gFID (Kouzelis et al., 2025; Yao & Wang, 2025). In this paper, we propose a remarkably simple variant of rFID that demonstrates strong correlation with gFID. Specifically, instead of directly evaluating the latents  $z^{(1:N)}$ , we consider linear interpolation between each latent  $z^{(i)}$  and its nearest neighbor element  $\text{NN}(z^{(i)})$  in the dataset within the latent space:

$$\begin{aligned} \text{iFID} &:= d_{\text{FID}}(x^{(1:N)}, g(\hat{z}^{(1:N)})), \text{ where } \hat{z}^{(i)} = \frac{1}{2}(z^{(i)} + \text{NN}(z^{(i)})), \\ \text{NN}(z^{(i)}) &:= \arg \min_{j=1, \dots, N} \|z^{(j)} - z^{(i)}\|. \end{aligned} \quad (6)$$

We refer to our metric as **interpolated FID (iFID)**, as iFID measures the sample quality of interpolated latents, rather than the quality of the latents themselves. In next sections, we first show that it is not accurate that rFID does not correlate to any kind of sample quality. In fact, rFID and iFID correlates to the sample quality of refinement and navigation phase respectively. Then, we explain why iFID correlates to diffusion sample quality while reconstruction metrics correlates negatively to diffusion sample quality, by connecting to diffusion generalization and hallucination literatures (Kamb & Ganguli, 2024; Niedoba et al., 2024; Abu-Hussein & Giryes, 2024; Song et al., 2025; Aithal et al., 2024).

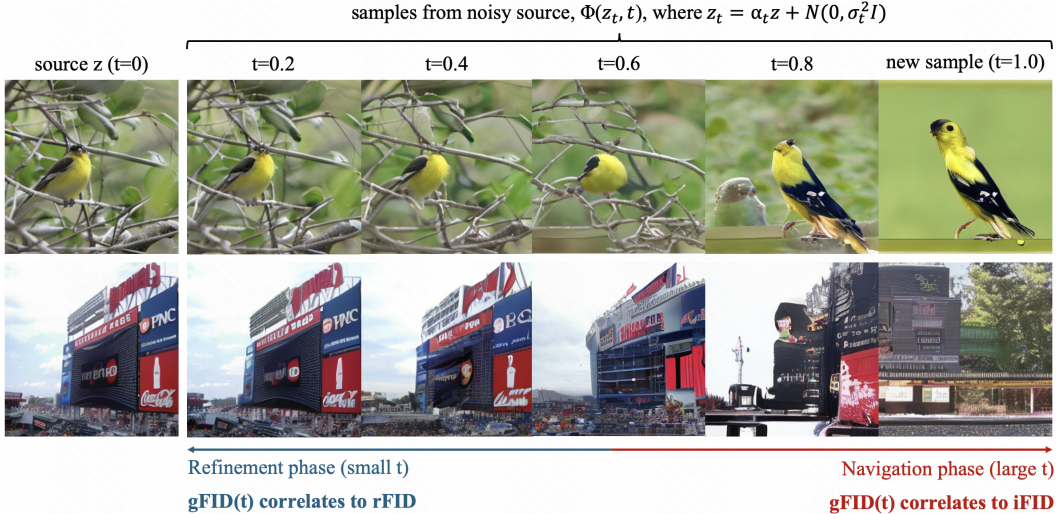


Figure 2: The refinement and navigation phases are key components of the sampling process for SiT-XL trained with SD-VAE. In the refinement phase (small  $t$ ), the sample generated from the noisy source is nearly identical to the source. In contrast, during the navigation phase (large  $t$ ), the sample from the noisy source differs significantly from the source.

Table 1: The Pearson Linear Correlation Coefficient (PCC) between rFID, iFID, and  $gFID(t)$  was analyzed. In the refinement phase of diffusion sampling (small  $t$ ), rFID exhibits a strong correlation with  $gFID(t)$ . In contrast, during the navigation phase of diffusion sampling (large  $t$ ), iFID demonstrates a higher correlation with  $gFID(t)$ .

	PCC with $gFID(t)$						
	t=0 (rFID)	t=0.1	t=0.2	t=0.4	t=0.6	t=0.8	t=1.0 (gFID)
	← Refinement phase			Navigation phase →			
rFID	1.00	0.37	0.20	-0.01	0.02	0.00	-0.06
iFID	0.06	0.26	0.67	0.69	0.77	0.85	0.89

### 3.3 RECONSTRUCTION FID AND INTERPOLATED FID PREDICTS SAMPLE QUALITY OF REFINEMENT AND NAVIGATION PHASE RESPECTIVELY

Previous works have shown that rFID does not correlate well with the quality of diffusion samples. In this work, we extend these findings by demonstrating that rFID correlates with diffusion sample quality during the refinement phase but not during the navigation phase. On the other hand, iFID correlates to the diffusion sample quality during the navigation phase but not during refinement phase.

As we have introduced before, refinement and navigation phase are two different stage of diffusion sampling process (Liu et al., 2025a; Song et al., 2025). So the sample quality in those two phases can not be separately evaluated directly. To separately measure the diffusion model’s abilities in the refinement and navigation phases, we follow (Song et al., 2025) and add noise to a source image, then denoise it using the diffusion model starting from an intermediate timestep  $t \in [0, T]$ . As  $t$  varies, the phenomena of refinement and navigation emerge: when  $t$  is small, the generated sample is almost identical to the source image, and the quality of these samples corresponds to the diffusion model’s sample quality in refinement phase. In contrast, when  $t$  is sufficiently large, the generated sample becomes quite different from the source image, and the quality of these samples reflects the model’s sample quality in navigation phase. Throughout this paper, we refer to the sample quality in the refinement and navigation phases as the quality of samples produced by adding noise to the source image and denoising from an intermediate timestep.

To quantify sample quality during the refinement and navigation phases, we extend the notion of gFID to  $\text{gFID}(t)$ , which is defined as the FID between the source image and diffusion samples generated from timestep  $t$ . Here, the starting point  $z_t^{(i)}$  is given by the image  $z^{(i)}$  and the forward diffusion process:

$$\text{gFID}(t) := d_{\text{FID}}(x^{(1:N)}, \Phi(z_t^{(1:N)}, t)), \text{ where } z_t^{(i)} \sim \mathcal{N}(\alpha_t z^{(i)}, \sigma_t^2 I). \quad (7)$$

It is evident that when  $t = 0$ ,  $\text{gFID}(t)$  reduces to rFID. As shown in Table 1, for a diffusion sampling trajectory with timestep  $t \in [0, 1]$ , rFID correlates strongly with  $\text{gFID}(t)$  in the refinement phase when  $t \leq 0.2$ . However, rFID does not correlate with  $\text{gFID}(t)$  in the navigation phase when  $t \geq 0.4$ .

On the other hand, iFID only correlates well with the sample quality during the navigation phase. As shown in Table 1, although iFID does not correlate with  $\text{gFID}(t)$  when  $t \leq 0.2$ , it correlates strongly with  $\text{gFID}(t)$  when  $t \geq 0.4$ . And clearly, iFID exhibits a strong correlation with the gFID of diffusion samples ( $\text{gFID}$  or  $\text{gFID}(1)$ ).

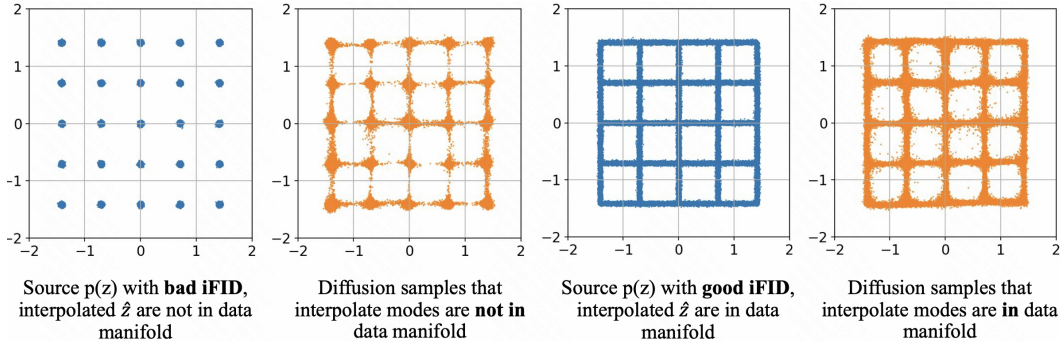


Figure 3: Toy example illustrating how different properties of the latent space lead to different diffusion sampling results. *Left two plots:* The latent is an isolated 25 Gaussian mixture in a two-dimensional square grid and exhibits poor iFID, since the interpolated  $\hat{z}$  does not lie on the data manifold. In this case, diffusion samples interpolating between nearby modes also fall outside the data manifold, leading to significant hallucination. *Right two plots:* The latent is a connected 25 Gaussian mixture and achieves good iFID, as the interpolated  $\hat{z}$  remains on the data manifold. Consequently, diffusion samples interpolating between nearby modes stay within the data manifold, and hallucination is reduced.

### 3.4 WHY INTERPOLATED FID PREDICTS SAMPLE QUALITY

**Diffusion Models Generate Unseen Samples by Interpolating Training Data** It is straightforward to understand why rFID predicts the sample quality during the refinement phase. After all, rFID is equivalent to  $\text{gFID}(0)$ , and when  $t$  is small,  $\text{gFID}(t)$  is close to  $\text{gFID}(0)$ . However, the reason why iFID predicts the final sample quality of diffusion model ( $\text{gFID}$  or  $\text{gFID}(1)$ ) is less obvious. To better understand why iFID is related to the sample quality of diffusion models, we first revisit the training objective of diffusion models. Specifically, for a fixed training dataset  $z^{(1:M)}$ , the score matching objective has a perfect solution known as the empirical score:

$$s_*(z_t, t) = \frac{1}{\sigma_t^2} (-z_t + \alpha_t \sum_{k=1}^M w_k(z_t) z^{(k)}),$$

$$\text{where } w_k(z_t) = \text{softmax}\left(\frac{\|z_t - \alpha_t z^{(k)}\|^2}{2\sigma_t^2}\right). \quad (8)$$

A well acknowledged result is, when the score estimator  $s_\theta(z_t, t)$  matches the empirical score  $s_*(z_t, t)$ , the diffusion model merely replicates samples from the training dataset (Kamb & Ganguli, 2024; Bonnaire et al., 2025b; Buchanan et al., 2025). Existing literature shows that the generalization ability of diffusion models, or their capacity to generate unseen samples, arises from underfitting (Kadkhodaie et al., 2023; Somepalli et al., 2022; Yoon et al., 2023; Buchanan et al.,

2025; Song et al., 2025): When  $t$  is large, the learned score deviate significantly from the empirical score due to the limited capacity of the neural network. This difference prevents diffusion models from replicating the training dataset.

How are the new samples related to the training dataset? Numerous studies have demonstrated that the new samples generated by diffusion models are interpolations and compositions of images from the training dataset (Okawa et al., 2023). Specifically, (Kamb & Ganguli, 2024; Somepalli et al., 2022) show that the new samples produced by diffusion models are local combinations of training samples. Furthermore, (Aithal et al., 2024; Deschenaux et al., 2024; Chandran.C et al., 2025) demonstrate that diffusion models interpolate between the modes of the training samples.

Although diffusion models can generate unseen samples by implicitly interpolating and composing images from training dataset, there is no guarantee on the quality of those samples. When the quality of those unseen sample is good, we say diffusion model generalizes (Kamb & Ganguli, 2024; Somepalli et al., 2022). While when the quality of those unseen sample is bad, we say diffusion model hallucinates (Deschenaux et al., 2024; Chandran.C et al., 2025).

**iFID Measures the Validity of Interpolated Data** Given the hypothesis that diffusion models generate new samples by interpolating and composing images from the training dataset, it follows intuitively that iFID correlates with the sample quality of diffusion model, as iFID measures the validity of interpolated latent representations. If iFID is 0, this indicates that the interpolated data share the same distribution as the source data, implying that the generated samples from diffusion models would also match the distribution of the source data, resulting in perfect generation. In other words, a latent space with a low iFID avoids hallucinations caused by mode interpolation (Aithal et al., 2024; Chandran.C et al., 2025).

**Toy Example with 2D Gaussian Mixture** To better illustrate the relationship between iFID and sample quality, we provide a toy example with two different types of latent space in Figure 3. First, we consider latent space with 25 isolated Gaussian mixture arranged in a two-dimensional square grid. Obviously this isolated latent has poor iFID as interpolated samples  $\hat{z}$  are not in data manifold. For isolated latent, many diffusion samples are interpolation of nearby modes. All those samples are also not in data manifold and becomes hallucination. On the other hand, the latent with 25 connected Gaussian mixture has good iFID as interpolated  $\hat{z}$  are in data manifold. And as the latent is already connected, the hallucination of diffusion samples is greatly alleviated.

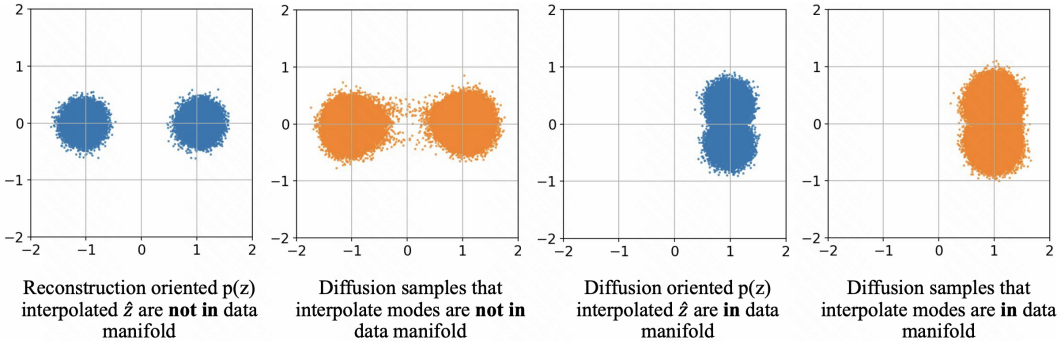


Figure 4: Toy example illustrating the difference between reconstruction-oriented latent and diffusion-oriented latent. *Left two plots:* The latent is an isolated 2-mode Gaussian mixture and exhibits poor interoperability, since the interpolated  $\hat{z}$  does not lie on the data manifold. In this case, diffusion samples interpolated between nearby modes also fall outside the data manifold, leading to hallucinations. *Right two plots:* The latent is an overlapping 2-mode Gaussian mixture with good interoperability, as the interpolated  $\hat{z}$  remains on the data manifold. Consequently, diffusion samples interpolated between nearby modes stay within the data manifold, and hallucinations are reduced.

### 3.5 WHY RECONSTRUCTION CORRELATES NEGATIVELY TO SAMPLE QUALITY

Based on previous findings that diffusion models prefer an interpolatable and connected latent space to generate valid unseen data, we can further explain why reconstruction metrics are often negatively correlated with diffusion sample quality. More specifically, the reconstruction metrics of VAEs fa-

vor an isolated and disconnected latent space. This is because an interpolatable and connected latent space is harder for the decoder to distinguish different inputs and thus leads to worse reconstruction performance. In contrast, a disconnected latent space is easier for the decoder to identify inputs, which results in better reconstruction. This leads to the so-called “reconstruction-generation dilemma” (Yao & Wang, 2025).

To clarify this intuition, we provide a toy example with two GMMs in Figure 4. Specifically, we consider a fully factorized Gaussian VAE trained on two data points  $x^{(1:2)}$ , with fixed posterior variance  $\sigma^2$  and KL divergence. We study the problem of optimizing the posterior mean  $\mu^{(i)}$  to minimize the reconstruction loss. To minimize the reconstruction error, the optimal strategy is to distribute  $\mu^{(i)}$  as separably as possible, allowing the decoder to easily associate each input  $x^{(i)}$  with its corresponding posterior sample  $z^{(i)}$ . However, such a separable latent space leads to hallucinations in diffusion models. As shown in Figure 4, the diffusion model interpolates between the two separable modes and those samples lie between the modes becomes hallucination. Conversely, if the latent modes exhibit significant overlap, hallucinations in diffusion models are reduced. Nevertheless, reconstruction becomes much more challenging, as the latent modes are no longer well-separated.

### 3.6 SUMMARY OF MAIN FINDINGS

- Contrary to previous assumptions, rFID does correlate with sample quality. Specifically, rFID is correlated with sample quality during the refinement phase, while iFID is correlated with sample quality during the navigation phase.
- iFID correlates with diffusion sample quality very well, because the diffusion model generates novel samples by interpolating between training data and iFID measures the validity of these interpolated samples.
- Reconstruction metrics are negatively correlated with diffusion sample quality, because reconstruction favor separable and disconnected latent while the diffusion model requires an interpolable and connected latent space to generate realistic unseen data.

Table 2: List of VAEs included in our study. We incorporate 13 VAEs with open-sourced models and train the corresponding diffusion models in their respective latent spaces.

VAE Name	Latent Dim.	Arch.	Training
SD-VAE (Rombach et al., 2022)	$4 \times 32 \times 32$	UNet	Recon.
IN-VAE (Yao & Wang, 2025)	$16 \times 16 \times 16$	UNet	Recon.
FLUX-VAE (Labs, 2024)	$16 \times 32 \times 32$	UNet	Recon.
QwenImage-VAE (Wu et al., 2025)	$16 \times 32 \times 32$	UNet	Recon.
SD3-VAE (Esser et al., 2024)	$16 \times 32 \times 32$	UNet	Recon.
EQ-VAE (Kouzelis et al., 2025)	$4 \times 32 \times 32$	UNet	Recon. + Equivariance
VA-VAE (Yao & Wang, 2025)	$16 \times 16 \times 16$	UNet	Recon. + DINO alignment
SOFT-VQ (Chen et al., 2025c)	$64 \times 32$	ViT	Recon. + DINO alignment
MAE-TOK (Chen et al., 2025b)	$128 \times 32$	ViT	Recon. + Mask + DINO alignment
DE-TOK (Yang et al., 2025)	$128 \times 32$	ViT	Recon. + Mask + latent denoising
DM-VAE (Ye et al., 2025)	$256 \times 32$	ViT	Recon. + Distribution Matching
REPAE-VAE (Leng et al., 2025)	$4 \times 32 \times 32$	UNet	Recon. + REPA Loss
RAE (Zheng et al., 2025)	$768 \times 16 \times 16$	ViT	DINO Encoder + Recon. Decoder

## 4 EXPERIMENTAL RESULTS

### 4.1 EXPERIMENT SETUP

**Dataset and Metrics** We conduct experiments on the  $256 \times 256$  ImageNet dataset. All diffusion models are trained on the ImageNet training split, and all metrics are evaluated on the ImageNet validation split. For reconstruction metrics, we consider PSNR, LPIPS, SSIM, and rFID, as these are standard metrics for evaluating VAEs. For non-reconstruction metrics, we consider diffusion loss and other loss functions designed to optimize VAEs for improved diffusion model performance, such as EQ Loss, SE Loss, VF Loss, and GMM Loss (Kouzelis et al., 2025; Skorokhodov et al., 2025; Yao & Wang, 2025; Chen et al., 2025a). To study the correlation of these metrics with the gFID of the diffusion model, we evaluate the Pearson correlation coefficient (PCC) and Spearman rank correlation coefficient (SRCC) between the metrics and gFID.

**VAE and Diffusion Models** We evaluate 13 VAEs with publicly available checkpoints; the details of these models are provided in Table 2. Some of these VAEs, such as SD-VAE, IN-VAE, QW-VAE, FLUX-VAE, and SD3-VAE (Rombach et al., 2022; Yao & Wang, 2025; Labs, 2024; Esser et al., 2024; Wu et al., 2025), are optimized solely for reconstruction. Some VAEs incorporate equivariance regularization, such as EQ-VAE (Kouzelis et al., 2025). Others employ contrastive learning-based image encoders, such as VA-VAE, SOFT-VQ, MAE-TOK, DE-TOK, DM-VAE, REPAE-VAE, and RAE (Yao & Wang, 2025; Chen et al., 2025c;a; Yang et al., 2025; Ye et al., 2025; Leng et al., 2025; Zheng et al., 2025). We include VAEs with diverse latent dimensions, ranging from the standard  $4 \times 32 \times 32$ , to large  $768 \times 16 \times 16$ , and even 1D latent  $128 \times 32$ . Furthermore, these VAEs also differ in model architecture, including both UNet and ViT models. We have not included some VAEs, such as Align-TOK, FLUX-SE, FAE, and FlatDINO (Chen et al., 2025a; Skorokhodov et al., 2025; Gao et al., 2025; Calvo-González & Fleuret, 2026), as no official checkpoints have been released for these models.

For all VAEs, we train two diffusion models of different sizes, SiT-B and SiT-XL, on their latent spaces. All diffusion models are trained using the Adam optimizer for 40 epochs. We evaluate gFID for both with and without classifier-free guidance (cfg).

Table 3: The correlation of different VAE metrics vs diffusion gFID. The correlation are computed on metrics collected by training SiT with 13 pre-trained VAEs. EQ Loss and SE Loss are not evaluated on VAE with 1D latent. RAE is not evaluated on SiT/B following (Zheng et al., 2025). PCC: Pearson correlation coefficient. SRCC: Spearman’s rank correlation coefficient. **Bold**: best.

Metrics	gFID SiT/B				gFID SiT/XL			
	w/o cfg		w/ cfg		w/o cfg		w/ cfg	
	PCC↑	SRCC↑	PCC↑	SRCC↑	PCC↑	SRCC↑	PCC↑	SRCC↑
<i>Reconstruction Metrics</i>								
-PSNR	-0.81	-0.81	-0.83	-0.82	-0.79	-0.78	-0.79	-0.85
-SSIM	-0.78	-0.81	-0.80	-0.84	-0.77	-0.78	-0.77	-0.85
LPIPS	-0.73	-0.74	-0.72	-0.76	-0.73	-0.72	-0.73	-0.79
rFID	-0.04	-0.31	-0.07	-0.31	-0.06	-0.21	-0.15	-0.31
<i>Non-reconstruction Metrics</i>								
Diffusion Loss	0.21	0.24	0.22	0.20	0.34	0.37	0.24	0.29
EQ Loss (Kouzelis et al., 2025)	-0.62	-0.52	-0.78	-0.76	-0.39	-0.15	-0.37	-0.13
SE Loss (Skorokhodov et al., 2025)	-0.70	-0.70	-0.75	-0.83	-0.77	-0.70	-0.79	-0.79
VF Loss (Yao & Wang, 2025)	0.10	0.05	0.09	0.03	0.17	0.11	0.09	-0.01
GMM Loss (Chen et al., 2025b)	0.25	0.04	0.25	0.05	0.28	0.01	0.23	-0.02
iFID (Ours)	<b>0.85</b>	<b>0.86</b>	<b>0.82</b>	<b>0.84</b>	<b>0.89</b>	<b>0.91</b>	<b>0.88</b>	<b>0.92</b>

## 4.2 MAIN RESULTS

**Reconstruction Metrics Correlate Negatively with Diffusion Sample Quality** As shown in Table 3, image-to-image distortion metrics, such as PSNR, SSIM, and LPIPS, are strongly negatively correlated with gFID. This result verifies the “reconstruction generation dilemma”, which states that the reconstruction performance of VAEs is at odds with the generation performance of diffusion models.

**iFID Exhibits Significantly Stronger Correlation with Diffusion Sample Quality** Among non-reconstruction metrics, several show reasonable positive correlations with gFID, such as diffusion loss, VF Loss (Yao & Wang, 2025), and GMM Loss (Chen et al., 2025a). However, our iFID demonstrates a significantly stronger correlation with gFID, achieving PCC and SRCC values around 0.9. It is also interesting to find that iFID has much stronger correlation to gFID than diffusion loss, which indicates that the diffusion loss might not be a strong signal for sample quality when latent space is different.

**Visualization of Nearest Neighbour and Interpolated Latent** In Figure 5, we visualize the decoded latent  $z$ , nearest neighbour latent  $NN(z)$  and the interpolated latent  $\hat{z}$  for different VAEs. It is shown that for reconstruction optimized VAEs, such as SD-VAE and FLUX-VAE (Rombach et al., 2022; Labs, 2024), the nearest neighbour latent  $NN(z)$  are often semantically irrelevant to  $z$ . Besides, the interpolated latent  $\hat{z}$  are invalid images. On the other hand, for diffusion optimized

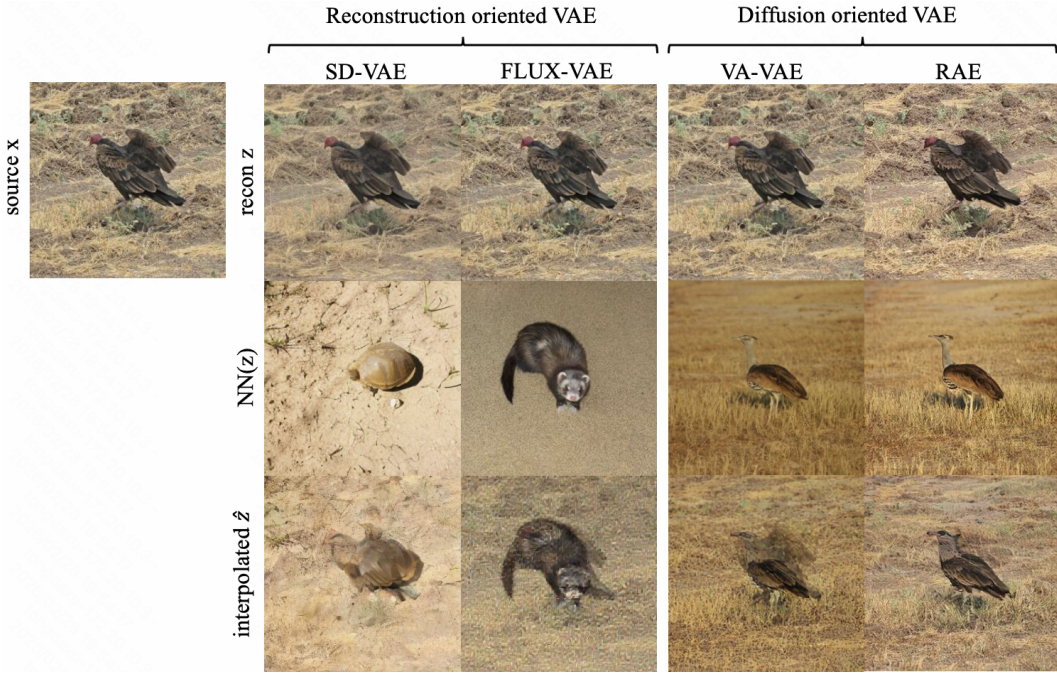


Figure 5: The visualization of decoded nearest neighbour latent  $NN(z)$  and the interpolated latent  $\hat{z}$ . For reconstruction oriented VAEs, the  $NN(z)$  is semantically different from  $z$ , and the interpolated  $\hat{z}$  are invalid images. While for diffusion oriented VAEs, the  $NN(z)$  is semantically similar to  $z$ , and the interpolated  $\hat{z}$  are realistic images.

VAEs, such as VA-VAE and RAE (Yao & Wang, 2025; Zheng et al., 2025), the nearest neighbour latent  $NN(z)$  are semantically similar to  $z$  and the interpolated latent  $\hat{z}$  are realistic images. Similar intuition is also shown by (Peng et al., 2022; Song et al., 2025).

### 4.3 SENSITIVITY ANALYSIS

We examine the alternatives and parameter choices involved in evaluating iFID. Note that our objective is not to select the best set of parameters, but rather to evaluate whether iFID is robust to different parameter selections.

**Interpolation Method and Strength** The choice of interpolation between  $z^{(i)}$  and its nearest neighbor image  $NN(z^{(i)})$  is intuitively important. The simplest interpolation method is linear interpolation. For Gaussian variational auto-encoders, spherical interpolation, which ensures that the interpolated images follow the Gaussian prior, is often considered a superior approach (Jang et al., 2024). Conversely, previous work on diffusion generalization (Kamb & Ganguli, 2024) suggests that random mask interpolation is also a reasonable choice. In Table 4, it is shown that spherical interpolation has the highest correlation with gFID. This indicates that preserving the Gaussian prior remains important for Gaussian VAEs. Nonetheless, both linear and mask interpolation also achieve high correlation (approximately 0.8).

By default, we set the interpolation strength of iFID to  $\alpha = 0.5$ , which represents the most challenging case. When  $\alpha = 0$ , the interpolated latent is identical to the source  $z$ , and iFID reduces to rFID. Conversely, when  $\alpha = 1$ , the interpolated latent is identical to  $NN(z)$ . As shown in Table 5, as  $\alpha$  increases from 0 to 0.5, the correlation of iFID with rFID decreases, while its correlation with gFID increases rapidly. When  $\alpha \geq 0.2$ , the correlation between iFID and gFID becomes reasonably high ( $\geq 0.6$ ).

**Reference Dataset Size** Intuitively, the number of images used to compute  $NN(\cdot)$  may influence the results. In practice, we use the 50k ImageNet validation set for  $z^{(i)}$ , and the 1000k ImageNet training set for computing  $NN(\cdot)$ . However, Table 4 shows that reducing the number of images used

for  $\text{NN}(\cdot)$  computation does not significantly affect the final results. In fact, using a 50k subset from the ImageNet training set already yields a satisfactory correlation (approximately 0.85).

**Top K Nearest Neighbor** It is natural to ask whether using the top  $K$  nearest neighbors significantly affects the results. In Table 4, we show that replacing the simple nearest neighbor with the top- $K$  nearest neighbors, where  $K = 10$ , has minimal impact on the correlation (PCC changes from 0.89 to 0.89 without cfg, and from 0.86 to 0.88 with cfg). The interpolation is achieved by randomly select one of those  $K$  latent.

Table 4: Sensitivity analysis on iFID’s latent interpolation method, number of images to compute nearest neighbour and  $K$  for top- $K$  nearest neighbour. iFID is robust to different parameters and shows consistent high correlation to gFID.

Interpolation	# of Images	$K$ for $\text{NN}(\cdot)$	gFID SiT-XL			
			w/o cfg		w/ cfg	
			PCC $\uparrow$	SRCC $\uparrow$	PCC $\uparrow$	SRCC $\uparrow$
Linear	50k	1	0.78	0.78	0.80	0.82
Mask	50k	1	0.74	0.77	0.75	0.76
Spherical	50k	1	0.84	0.85	0.86	0.81
Spherical	200k	1	0.88	0.89	0.86	0.87
Spherical	1000k	1	0.89	0.89	0.86	0.87
Spherical	1000k	10	0.89	0.91	0.88	0.92

Table 5: Sensitivity analysis on iFID’s latent interpolation strength  $\alpha$ . It is shown that as  $\alpha$  grows from 0 to 0.5, iFID correlates more to gFID and less to rFID. And the correlation becomes reasonably strong when  $\alpha \geq 0.2$ .

Interpolation strength $\alpha$	rFID		gFID SiT-XL			
			w/o cfg		w/ cfg	
	PCC $\uparrow$	SRCC $\uparrow$	PCC $\uparrow$	SRCC $\uparrow$	PCC $\uparrow$	SRCC $\uparrow$
$\alpha = 0.0$ (rFID)	1.00	1.00	-0.06	-0.21	-0.15	-0.31
$\alpha = 0.1$	0.21	0.67	0.37	0.22	0.38	0.36
$\alpha = 0.2$	-0.14	0.14	0.63	0.53	0.62	0.52
$\alpha = 0.3$	-0.14	0.11	0.66	0.59	0.65	0.58
$\alpha = 0.4$	0.00	0.19	0.78	0.79	0.76	0.79
$\alpha = 0.5$ (iFID)	0.06	0.10	0.89	0.91	0.88	0.92

## 5 RELATED WORKS

### 5.1 VARIATIONAL AUTOENCODERS FOR DIFFUSION MODELS

In early works on latent diffusion models, VAEs are trained solely to optimize reconstruction metrics (Rombach et al., 2022; Esser et al., 2024). It may seem intuitive that VAEs with better reconstruction capture more details and thus facilitate the training of better generative models. However, later studies reveal that standard reconstruction-based optimization does not benefit diffusion sampling, and this phenomena is known as “reconstruction-generation dilemma”. (Wehenkel & Louppe, 2021; Vahdat et al., 2021; Heek et al., 2026) propose training VAEs with a diffusion prior to improve diffusion models. (Kouzelis et al., 2025; Skorokhodov et al., 2025; Liu et al., 2025b; Fan et al., 2025) explains and regularize VAEs from signal processing perspective. Additionally, (Chen et al., 2025c;b; Zheng et al., 2025; Yao & Wang, 2025; Ye et al., 2025; Yang et al., 2025; Yao et al., 2025; Shi et al., 2025; Gao et al., 2025) propose connecting VAE to contrastive learning based image encoders such as DINO and MAE (Oquab et al., 2023; He et al., 2022).

Despite recent advances in VAEs, effective metrics for measuring their diffusability, and explanation on why “reconstruction-generation dilemma” happens remain underexplored. The regularization losses in these VAEs, such as the VF Loss (Yao & Wang, 2025) and EQ Loss (Kouzelis et al., 2025), can be directly used as metrics; however, their correlation with gFID is weak. (He et al.,

2022) propose using the GMM Loss of the latent space as a metric, and find a strong correlation in four VAEs, including vanilla auto-encoder, SD-VAE, VA-VAE and MAE-TOK (Rombach et al., 2022; Yao & Wang, 2025; Chen et al., 2025b). However, the correlation diminishes when evaluated on more VAEs as shown in Table 3. (Leng et al., 2025) introduce a metric to predict gFID, but it requires the training of a diffusion model. In this paper, we propose the first metric that correlates well with the gFID of diffusion. Additionally, we explain why iFID succeeds whereas reconstruction metrics fail to predict gFID, by linking our results to findings in the diffusion generalization and hallucination literature. A potential connection between nearest neighbor elements in the latent space and generation performance has been suggested for years (Peng et al., 2022; Song et al., 2025); however, we are the first to quantitatively study this relationship.

## 5.2 HOW DIFFUSION MODELS GENERATE UNSEEN SAMPLES

How diffusion models generate unseen samples is a fundamental question. In general, it is believed that underfitting, under-parameterization, and inductive bias in the score estimator lead to deviations of the learned score from the empirical score (Scarvelis et al., 2023; Kadkhodaie et al., 2023; Kamb & Ganguli, 2024; Bonnaire et al., 2025b;a; Song et al., 2025). Such deviations prevent diffusion models from replicating the training data. (Kamb & Ganguli, 2024; Niedoba et al., 2024; Okawa et al., 2023; Deschenaux et al., 2024) argue that diffusion models generate novel samples by composing and interpolating images from training dataset. Similarly, (Zhang et al., 2025) demonstrate that diffusion models generalize by linear interpolation in the latent space of the score matching network. Conversely, (Aithal et al., 2024; Chandran.C et al., 2025; Baptista et al., 2025) show that diffusion models can generate invalid samples, or hallucinate, by interpolating between nearby modes of the training data. Inspired by these findings in diffusion generalization and hallucination, we demonstrate that iFID strongly correlates with gFID, as it measures the validity of interpolated samples, and that reconstruction negatively correlates with gFID, as it favors a separable latent space.

## 5.3 DISCUSSION & CONCLUSION

Although iFID is strongly correlated with the gFID of diffusion models, there is no straightforward way to minimize it, especially when the dimension of the latent space is high (Palma et al., 2025). A possible method to optimize iFID may involve manifold sharpness (Jeon et al., 2024), which we leave for future work.

In conclusion, we propose interpolated FID (iFID), a simple variant of rFID that is strongly correlated with the diffusion generation FID. Our key findings are as follows: rFID correlates with sample quality in the refinement phase, while iFID correlates with sample quality in the navigation phase; iFID correlates with gFID because diffusion models generate unseen samples by interpolating training images, and iFID measures the quality of these interpolated images; reconstruction metrics negatively correlate with generation because reconstruction favors disconnected latents, whereas generation favors interpolatable latents. To our knowledge, iFID is the first metric that is strongly correlated with diffusion gFID across diverse VAEs.

## REFERENCES

- Shady Abu-Hussein and Raja Giryes. Udp: Upsampling diffusion probabilistic models. *Advances in Neural Information Processing Systems*, 37:27616–27646, 2024.
- Sumukh K Aithal, Pratyush Maini, Zachary Chase Lipton, and J. Zico Kolter. Understanding hallucinations in diffusion models through mode interpolation. *ArXiv*, abs/2406.09358, 2024. URL <https://api.semanticscholar.org/CorpusID:270440527>.
- Brian D. O. Anderson. Reverse-time diffusion equation models. *Stochastic Processes and their Applications*, 12:313–326, 1982. URL <https://api.semanticscholar.org/CorpusID:3897405>.
- Ricardo Baptista, Agnimitra Dasgupta, Nikola B Kovachki, Assad Oberai, and Andrew M Stuart. Memorization and regularization in generative diffusion models. *arXiv preprint arXiv:2501.15785*, 2025.

- Tony Bonnaire, Raphaël Urfin, Giulio Biroli, and Marc Mézard. Why diffusion models don't memorize: The role of implicit dynamical regularization in training. *arXiv preprint arXiv:2505.17638*, 2025a.
- Tony Bonnaire, Raphaël Urfin, Giulio Biroli, and Marc Mézard. Why Diffusion Models Don't Memorize: The Role of Implicit Dynamical Regularization in Training. 10 2025b. URL <http://arxiv.org/abs/2505.17638>.
- Sam Buchanan, Druv Pai, Yi Ma, and Valentin De Bortoli. On the edge of memorization in diffusion models. *ArXiv*, abs/2508.17689, 2025. URL <https://api.semanticscholar.org/CorpusID:280711597>.
- Ram'on Calvo-Gonz'alez and Francois Fleuret. Laminating representation autoencoders for efficient diffusion. 2026. URL <https://api.semanticscholar.org/CorpusID:285285751>.
- Barath Chandran, C. Srinivas Anumasa, and Dianbo Liu. Laplacian score sharpening for mitigating hallucination in diffusion models. *ArXiv*, abs/2511.07496, 2025. URL <https://api.semanticscholar.org/CorpusID:282922289>.
- Bowei Chen, Sai Bi, Hao Tan, He Zhang, Tianyuan Zhang, Zhengqi Li, Yuanjun Xiong, Jianming Zhang, and Kai Zhang. Aligning visual foundation encoders to tokenizers for diffusion models. *arXiv preprint arXiv:2509.25162*, 2025a.
- Hao Chen, Yujin Han, Fangyi Chen, Xiang Li, Yidong Wang, Jindong Wang, Ze Wang, Zicheng Liu, Difan Zou, and Bhiksha Raj. Masked autoencoders are effective tokenizers for diffusion models. *ArXiv*, abs/2502.03444, 2025b. URL <https://api.semanticscholar.org/CorpusID:276116849>.
- Hao Chen, Ze Wang, Xiang Li, Ximeng Sun, Fangyi Chen, Jiang Liu, Jindong Wang, Bhiksha Raj, Zicheng Liu, and Emad Barsoum. Softvq-vae: Efficient 1-dimensional continuous tokenizer. In *Proceedings of the Computer Vision and Pattern Recognition Conference*, pp. 28358–28370, 2025c.
- Justin Deschenaux, Igor Krawczuk, Grigorios G. Chrysos, and Volkan Cevher. Going beyond compositions, ddpms can produce zero-shot interpolations. In *International Conference on Machine Learning*, 2024. URL <https://api.semanticscholar.org/CorpusID:270095412>.
- Patrick Esser, Sumith Kulal, Andreas Blattmann, Rahim Entezari, Jonas Müller, Harry Saini, Yam Levi, Dominik Lorenz, Axel Sauer, Frederic Boesel, et al. Scaling rectified flow transformers for high-resolution image synthesis. In *Forty-first international conference on machine learning*, 2024.
- Weichen Fan, Haiwen Diao, Quan Wang, Dahua Lin, and Ziwei Liu. The prism hypothesis: Harmonizing semantic and pixel representations via unified autoencoding. *arXiv preprint arXiv:2512.19693*, 2025.
- Yuan Gao, Chen Chen, Tianrong Chen, and Jiatao Gu. One layer is enough: Adapting pretrained visual encoders for image generation. *ArXiv*, abs/2512.07829, 2025. URL <https://api.semanticscholar.org/CorpusID:283694483>.
- Kristian Georgiev, Joshua Vendrow, Hadi Salman, Sung Min Park, and Aleksander Madry. The journey, not the destination: How data guides diffusion models. *ArXiv*, abs/2312.06205, 2023. URL <https://api.semanticscholar.org/CorpusID:266162342>.
- Kaiming He, Xinlei Chen, Saining Xie, Yanghao Li, Piotr Dollár, and Ross Girshick. Masked autoencoders are scalable vision learners. In *Proceedings of the IEEE/CVF conference on computer vision and pattern recognition*, pp. 16000–16009, 2022.
- Jonathan Heek, Emiel Hoogeboom, Thomas Mensink, and Tim Salimans. Unified latents (ul): How to train your latents. 2026. URL <https://api.semanticscholar.org/CorpusID:285787616>.

- Martin Heusel, Hubert Ramsauer, Thomas Unterthiner, Bernhard Nessler, and Sepp Hochreiter. Gans trained by a two time-scale update rule converge to a local nash equilibrium. In *Neural Information Processing Systems*, 2017. URL <https://api.semanticscholar.org/CorpusID:326772>.
- Jonathan Ho, Ajay Jain, and P. Abbeel. Denoising diffusion probabilistic models. *ArXiv*, abs/2006.11239, 2020. URL <https://api.semanticscholar.org/CorpusID:219955663>.
- Young Kyun Jang, Dat Huynh, Ashish Shah, Wenkang Chen, and Ser-Nam Lim. Spherical linear interpolation and text-anchoring for zero-shot composed image retrieval. *ArXiv*, abs/2405.00571, 2024. URL <https://api.semanticscholar.org/CorpusID:269484503>.
- Dongjae Jeon, Dueun Kim, and Albert No. Understanding and mitigating memorization in generative models via sharpness of probability landscapes. In *International Conference on Machine Learning*, 2024. URL <https://api.semanticscholar.org/CorpusID:274515202>.
- Zahra Kadkhodaie, Florentin Guth, Eero P. Simoncelli, and St'ephane Mallat. Generalization in diffusion models arises from geometry-adaptive harmonic representation. *ArXiv*, abs/2310.02557, 2023. URL <https://api.semanticscholar.org/CorpusID:263620724>.
- Mason Kamb and Surya Ganguli. An analytic theory of creativity in convolutional diffusion models. *ArXiv*, abs/2412.20292, 2024. URL <https://api.semanticscholar.org/CorpusID:275134200>.
- Diederik P. Kingma and Max Welling. Auto-encoding variational bayes. *CoRR*, abs/1312.6114, 2013. URL <https://api.semanticscholar.org/CorpusID:216078090>.
- Theodoros Kouzelis, Ioannis Kakogeorgiou, Spyros Gidaris, and Nikos Komodakis. Eq-vae: Equivariance regularized latent space for improved generative image modeling. *ArXiv*, abs/2502.09509, 2025. URL <https://api.semanticscholar.org/CorpusID:276317789>.
- Black Forest Labs. Flux. <https://github.com/black-forest-labs/flux>, 2024.
- Xingjian Leng, Jaskirat Singh, Yunzhong Hou, Zhenchang Xing, Saining Xie, and Liang Zheng. Repa-e: Unlocking vae for end-to-end tuning with latent diffusion transformers. *ArXiv*, abs/2504.10483, 2025. URL <https://api.semanticscholar.org/CorpusID:277781071>.
- Marvin Li and Sitan Chen. Critical windows: non-asymptotic theory for feature emergence in diffusion models. *ArXiv*, abs/2403.01633, 2024. URL <https://api.semanticscholar.org/CorpusID:268247745>.
- Haoming Liu, Jinnuo Liu, Yanhao Li, Liuyang Bai, Yunkai Ji, Yuanhe Guo, Shenji Wan, and Hongyi Wen. From navigation to refinement: Revealing the two-stage nature of flow-based diffusion models through oracle velocity. *ArXiv*, abs/2512.02826, 2025a. URL <https://api.semanticscholar.org/CorpusID:283458653>.
- Shizhan Liu, Xinran Deng, Zhuoyi Yang, Jiayan Teng, Xiaotao Gu, and Jie Tang. Delving into latent spectral biasing of video vaes for superior diffusability. *arXiv preprint arXiv:2512.05394*, 2025b.
- Matthew Niedoba, Berend Zwartsenberg, Kevin Murphy, and Frank Wood. Towards a mechanistic explanation of diffusion model generalization. *arXiv preprint arXiv:2411.19339*, 2024.
- Maya Okawa, Ekdeep Singh Lubana, Robert P. Dick, and Hidenori Tanaka. Compositional abilities emerge multiplicatively: Exploring diffusion models on a synthetic task. *ArXiv*, abs/2310.09336, 2023. URL <https://api.semanticscholar.org/CorpusID:264146105>.
- Maxime Oquab, Timothée Darcet, Théo Moutakanni, Huy Vo, Marc Szafraniec, Vasil Khalidov, Pierre Fernandez, Daniel Haziza, Francisco Massa, Alaaeldin El-Nouby, et al. Dinov2: Learning robust visual features without supervision. *arXiv preprint arXiv:2304.07193*, 2023.

- Alessandro Palma, Sergei Rybakov, Leon Hetzel, Stephan Günnemann, and Fabian J Theis. Enforcing latent euclidean geometry in single-cell vaes for manifold interpolation. *arXiv preprint arXiv:2507.11789*, 2025.
- Zhiliang Peng, Li Dong, Hangbo Bao, Qixiang Ye, and Furu Wei. Beit v2: Masked image modeling with vector-quantized visual tokenizers. *arXiv preprint arXiv:2208.06366*, 2022.
- Robin Rombach, Andreas Blattmann, Dominik Lorenz, Patrick Esser, and Björn Ommer. High-resolution image synthesis with latent diffusion models. In *Proceedings of the IEEE/CVF conference on computer vision and pattern recognition*, pp. 10684–10695, 2022.
- Christopher Scarvelis, Haitz S’aez de Oc’ariz Borde, and Justin Solomon. Closed-form diffusion models. *ArXiv*, abs/2310.12395, 2023. URL <https://api.semanticscholar.org/CorpusID:264305821>.
- Minglei Shi, Haolin Wang, Wenzhao Zheng, Ziyang Yuan, Xiaoshi Wu, Xintao Wang, Pengfei Wan, Jie Zhou, and Jiwen Lu. Latent diffusion model without variational autoencoder. *ArXiv*, abs/2510.15301, 2025. URL <https://api.semanticscholar.org/CorpusID:282203316>.
- Ivan Skorokhodov, Sharath Girish, Benran Hu, Willi Menapace, Yanyu Li, Rameen Abdal, Sergey Tulyakov, and Aliaksandr Siarohin. Improving the diffusability of autoencoders. *ArXiv*, abs/2502.14831, 2025. URL <https://api.semanticscholar.org/CorpusID:276482178>.
- Gowthami Somepalli, Vasu Singla, Micah Goldblum, Jonas Geiping, and Tom Goldstein. Diffusion art or digital forgery? investigating data replication in diffusion models. *2023 IEEE/CVF Conference on Computer Vision and Pattern Recognition (CVPR)*, pp. 6048–6058, 2022. URL <https://api.semanticscholar.org/CorpusID:254366634>.
- Kiwhan Song, Jaeyeon Kim, Sitan Chen, Yilun Du, Sham M. Kakade, and Vincent Sitzmann. Selective underfitting in diffusion models. *ArXiv*, abs/2510.01378, 2025. URL <https://api.semanticscholar.org/CorpusID:281724714>.
- Yang Song, Jascha Narain Sohl-Dickstein, Diederik P. Kingma, Abhishek Kumar, Stefano Ermon, and Ben Poole. Score-based generative modeling through stochastic differential equations. *ArXiv*, abs/2011.13456, 2020. URL <https://api.semanticscholar.org/CorpusID:227209335>.
- Arash Vahdat, Karsten Kreis, and Jan Kautz. Score-based generative modeling in latent space, 2021. URL <https://arxiv.org/abs/2106.05931>, 2021.
- Pascal Vincent. A connection between score matching and denoising autoencoders. *Neural Computation*, 23:1661–1674, 2011. URL <https://api.semanticscholar.org/CorpusID:5560643>.
- Antoine Wehenkel and Gilles Louppe. Diffusion priors in variational autoencoders. *arXiv preprint arXiv:2106.15671*, 2021.
- Chenfei Wu, Jiahao Li, Jingren Zhou, Junyang Lin, Kaiyuan Gao, Kun Yan, Sheng-ming Yin, Shuai Bai, Xiao Xu, Yilei Chen, et al. Qwen-image technical report. *arXiv preprint arXiv:2508.02324*, 2025.
- Jiawei Yang, Tianhong Li, Lijie Fan, Yonglong Tian, and Yue Wang. Latent denoising makes good visual tokenizers. *arXiv preprint arXiv:2507.15856*, 2025.
- Jingfeng Yao and Xinggang Wang. Reconstruction vs. generation: Taming optimization dilemma in latent diffusion models. *2025 IEEE/CVF Conference on Computer Vision and Pattern Recognition (CVPR)*, pp. 15703–15712, 2025. URL <https://api.semanticscholar.org/CorpusID:275211938>.
- Jingfeng Yao, Yuda Song, Yucong Zhou, and Xinggang Wang. Towards scalable pre-training of visual tokenizers for generation. *arXiv preprint arXiv:2512.13687*, 2025.

Sen Ye, Jianning Pei, Mengde Xu, Shuyang Gu, Chunyu Wang, Liwei Wang, and Han Hu. Distribution matching variational autoencoder. *arXiv preprint arXiv:2512.07778*, 2025.

Taeho Yoon, Joo Young Choi, Sehyun Kwon, and Ernest K Ryu. Diffusion Probabilistic Models Generalize when They Fail to Memorize. Technical report, 2023.

Zekai Zhang, Xiao Li, Xiang Li, Lianghe Shi, Meng Wu, Molei Tao, and Qing Qu. Generalization of diffusion models arises with a balanced representation space. *ArXiv*, abs/2512.20963, 2025. URL <https://api.semanticscholar.org/CorpusID:284153760>.

Boyang Zheng, Nanye Ma, Shengbang Tong, and Saining Xie. Diffusion transformers with representation autoencoders. *arXiv preprint arXiv:2510.11690*, 2025.

## A ADDITIONAL EXPERIMENTAL RESULTS

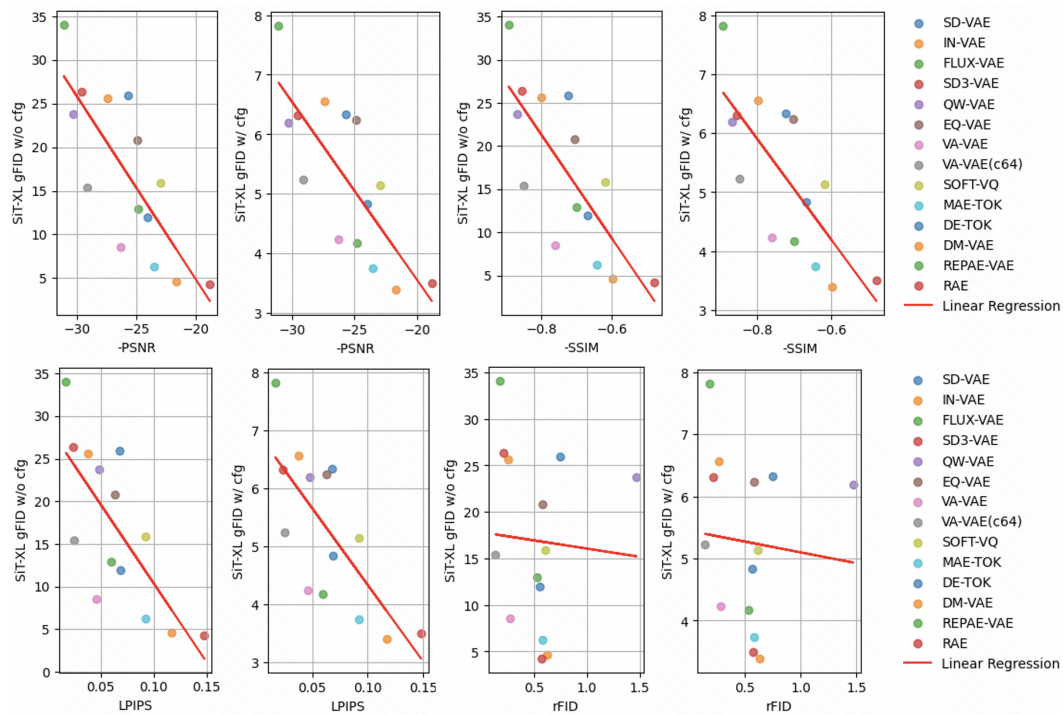


Figure 6: The relationship between reconstruction metrics and gFID for SiT/XL. It is shown that reconstruction metrics are often negatively correlated with gFID.

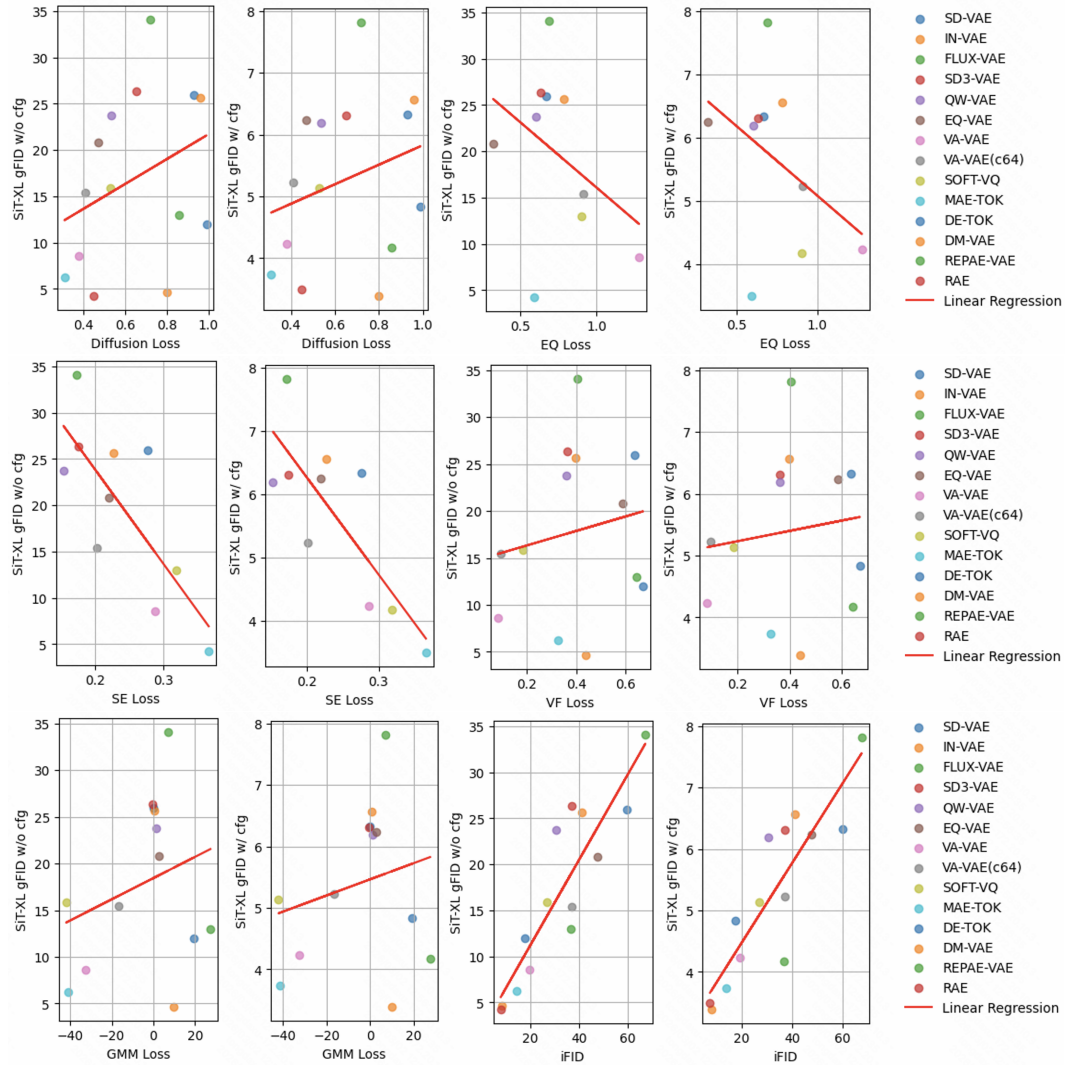


Figure 7: The relationship between non-reconstruction metrics and gFID for SiT/XL. It is shown our iFID is the only metric which is strongly correlated with gFID.